NANO LETTERS

2001
Vol. 1, No. 11
637−642

Supramolecular Templating of Thermally Stable Crystalline Mesoporous Metal Oxides Using Nanoparticulate Precursors

Michael S. Wong,† Esther S. Jeng, and Jackie Y. Ying*

Department of Chemical Engineering, Massachusetts Institute of Technology, Cambridge, Massachusetts 02139-4307

Received August 1, 2001

ABSTRACT

A supramolecular templating approach to the preparation of crystalline mesoporous metal oxides using inorganic colloidal nanoparticles as building blocks is presented. The nanoparticles are used to form a mesostructured material with a triblock copolymer surfactant as the templating agent and with a tungstate salt as the "binding" agent. Tungstated zirconium oxide produced in this manner was found to be highly thermally stable (in excess of 600 °C) while maintaining mesoporosity and a high surface area. Other mesoporous oxides were produced using zirconium salts, titania nanoparticles, and aluminum polycations, illustrating the flexibility of this "nanoparticle/surfactant templating" route.

MCM-41 and other M41S mesoporous silicates were the first example of supramolecular templating as a materials design strategy, in which aggregates of amphiphilic molecules were used to organize inorganic molecular precursors into a highly ordered organic−inorganic mesostructure.[1] The mesoporous material is obtained after removing the organics from the mesostructure. Subsequent advances in supramolecular templating have led to the preparation of mesoporous materials with new compositions and structures.[2] Pure silica and doped silicate mesoporous materials have high surface areas (>1000 m^2/g), controllable uniform pore sizes (2−10 nm), high pore volumes (>1 cm^3/g), ordered pore structures, and thermal stabilities in excess of 800 °C.[1,3−6] With their high degree of processibility (into powders, fibers, films, etc.) and rich surface chemistry, mesoporous silicates have great promise in applications as diverse as catalysis, separations, sensors, and optoelectronics.[7,8]

Mesoporous materials can also be prepared with non-silicate compositions, such as titania,[9] niobia,[10a−b] tantala,[10c] mixed metal oxides,[11] and phosphates of zirconia[12,13] and alumina.[14] These materials have structural properties similar to those of the mesoporous silicates, but the resulting surface areas and thermal stabilities are generally lower. The lower thermal stability hinders the development of mesoporous non-silicates for applications that require robustness and non-silicate surface chemistries, such as petroleum refining catalytic processes.[15]

A number of methods have been used to strengthen the non-silicate pore walls. Porous materials were found by using silica as a co-support in a niobium−tungsten oxide framework;[16] by attaching anionic species, such as phosphates and sulfates, to the zirconia pore wall surface;[12,13] by hydrothermally treating a surfactant-containing titania−zirconia mesostructure to crystallize the titania component before calcination;[17] and by synthesizing mesostructures with walls thick enough to allow partial crystallization without pore collapse.[11] Despite all these efforts, the resulting materials were mostly less thermally stable than mesoporous silicates.

In this letter, we present the novel use of nanoparticulate precursors in supramolecular templating as a means to promote the stability of non-silicate mesoporous materials. Mesoporous tungstated zirconium oxide with high thermal stability was synthesized with zirconia nanoparticles, a polymer surfactant, and a tungstate salt. The structural properties were characterized through transmission electron microscopy (TEM), X-ray diffractometry (XRD), small-angle X-ray scattering (SAXS), nitrogen adsorption, and differential thermal analysis (DTA). A nanoparticle/surfactant templating route was proposed to be based on attractive charge and hydrogen-bonding interactions.

For the synthesis of mesoporous tungstated zirconia, designated as WZr-TMS14, 14.3 g of a solution of 5.7 wt % Pluronic P123 surfactant (MW ∼ 5750, BASF) were prepared. This surfactant is a nonionic poly(ethylene oxide)−

* To whom correspondence should be addressed. Tel: +1-617-253-2899. Fax: +1-617-258-5766. E-mail: jyying@mit.edu.
† Present Address: Department of Chemical Engineering, Rice University, Houston, Texas 77005-1892.

10.1021/nl015594y CCC: $20.00
Published on Web 10/12/2001

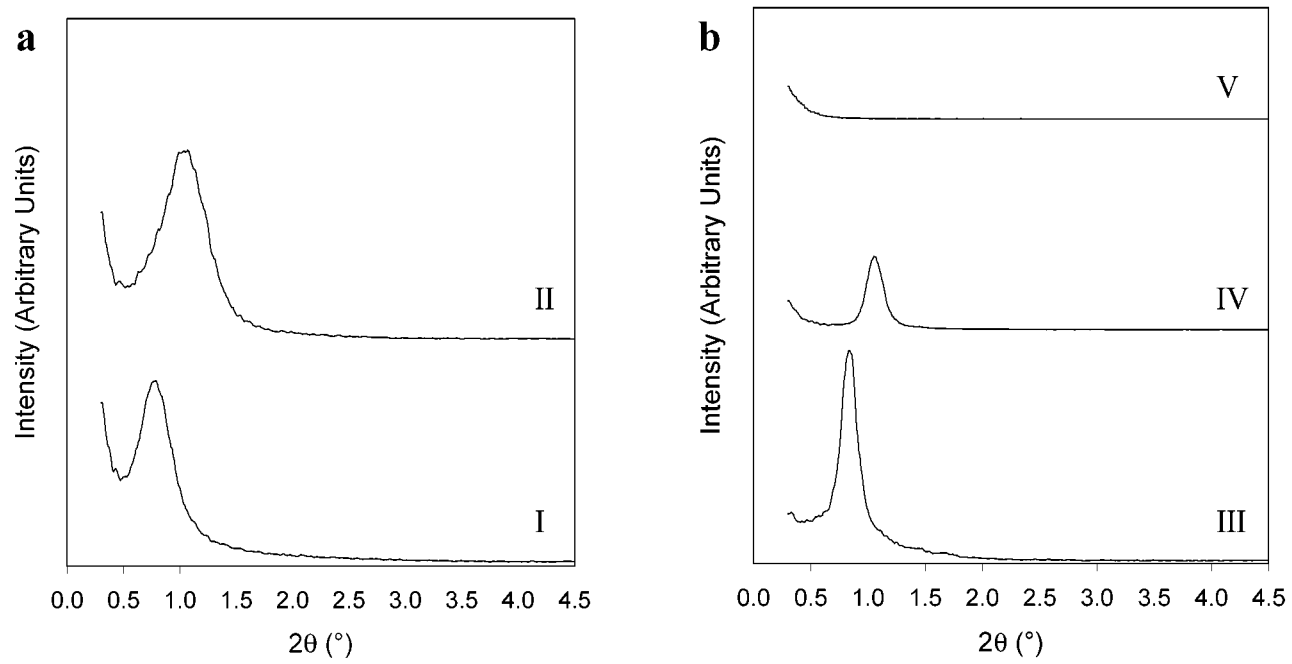

Figure 1. SAXS patterns of WZr-TMS14 prepared with (a) colloidal ZrO_2 nanoparticles and (b) with $ZrO(NO_3)_2$ salt. Traces I and III are patterns for the as-synthesized materials. Traces II and V are patterns for those materials calcined at 600 °C under air. Trace IV is the SAXS pattern for WZr-TMS14 prepared with $ZrO(NO_3)_2$ salt precursor and calcined to 250 °C under nitrogen. The SAXS patterns were collected using a Siemens small-angle diffractometer with a Siemens HI−STAR area detector, operating at 40 kV and 30 mA ($\lambda = 1.5406$ Å).

poly(propylene oxide)−poly(ethylene oxide) triblock copolymer with the structural formula $(EO)_x(PO)_y(EO)_x$, where $x = 20$, $y = 70$. 0.81 g of ammonium metatungstate ($(NH_4)_6H_2W_{12}O_{40}$ or "AWO," Strem) was then added to this surfactant solution. While this clear solution was stirring, 8.1 g of a 20 wt % zirconium oxide colloid sol (Nyacol Zr10/20, pH ∼ 0.5, PQ Corp.) were quickly added. Particle sizes of the zirconia precursor were reported by the commercial supplier to be nominally 5−10 nm but were found to be as small as 3 nm through high-resolution TEM. The final weight ratio of the synthesis mixture was 1 ZrO_2:0.5 AWO:0.5 Pluronic:11.9 H_2O. Immediate precipitation resulted, and after stirring for 2 h, the mixture was left to age for 2 days at room temperature. A white precipitate was recovered through washing with water and centrifuging, followed by decanting the supernatant; this procedure was repeated three times. The collected material was left to dry in air overnight, and then ground into a fine powder. Calcination under flowing air in a quartz tube at 600 °C for 3 h (ramp rate = 3.2 °C/min) resulted in a white powder.

WZr-TMS14 exhibited a low-angle scattering maximum in its SAXS pattern before and after calcination at 600 °C (Figure 1a). The main peak shown in Figure 1a represents an average scattering distance between the inorganic walls, which can be calculated from Bragg's law. The Bragg spacing of WZr-TMS14 decreased by 25% from 11.5 to 8.6 nm upon calcination, indicating that the inorganic framework contracted significantly without structural collapse. The main scattering peak was broad, and there were no higher-order scattering peaks that indicated any highly ordered pore structure. WZr-TMS14 did not show any wide-angle XRD peaks before and after calcination at 600 °C, indicating that either the material was completely amorphous or it contained crystalline domains too small to detect through XRD.

Calcined WZr-TMS14 was found to have a highly porous structure (Figure 2a). The pores appeared to be interconnected and to have a wormlike character. WZr-TMS14 resembled various disordered supramolecular-templated silicates,[6,18] but its pores were much larger and the pore walls were thicker. The Type IV nitrogen adsorption-desorption isotherm of WZr-TMS14 is representative of materials containing mesopores (Figure 3). The calculated pore size distribution (inset, Figure 3) matched well with the pore diameter (4−7 nm) measured from TEM. The pore wall thickness of WZr-TMS14 was observed to be about 4−6 nm (Figure 2b), suggesting the pore wall thickness was roughly defined by the precursor nanoparticle size. Indeed, crystalline grains of zirconia (∼4 ± 1 nm, Figure 2b) were observed within the pore walls and throughout the WZr-TMS14 particles. Electron diffraction analysis revealed two diffuse diffraction rings (Figure 2c), which can be assigned unequivocally to the cubic phase of zirconia, the same phase as the zirconia nanoparticle precursor (Figure 2d). The diffuseness may be due to partial amorphization of the zirconia particles by surface-bound tungstate species, a phenomenon seen in tungstate−alumina systems.[19] It is concluded that WZr-TMS14 exhibited nanocrystallinity in its pore walls. Both the particle size and crystal phase of the nanoparticle precursor were found substantially preserved in the mesoporous material.

DTA results showed that WZr-TMS14 was stable to very high temperatures (Figure 4a). An exothermic peak in the DTA profile of 600 °C-calcined WZr-TMS14 was found at 715 °C. This crystallization event destroyed the mesoporous

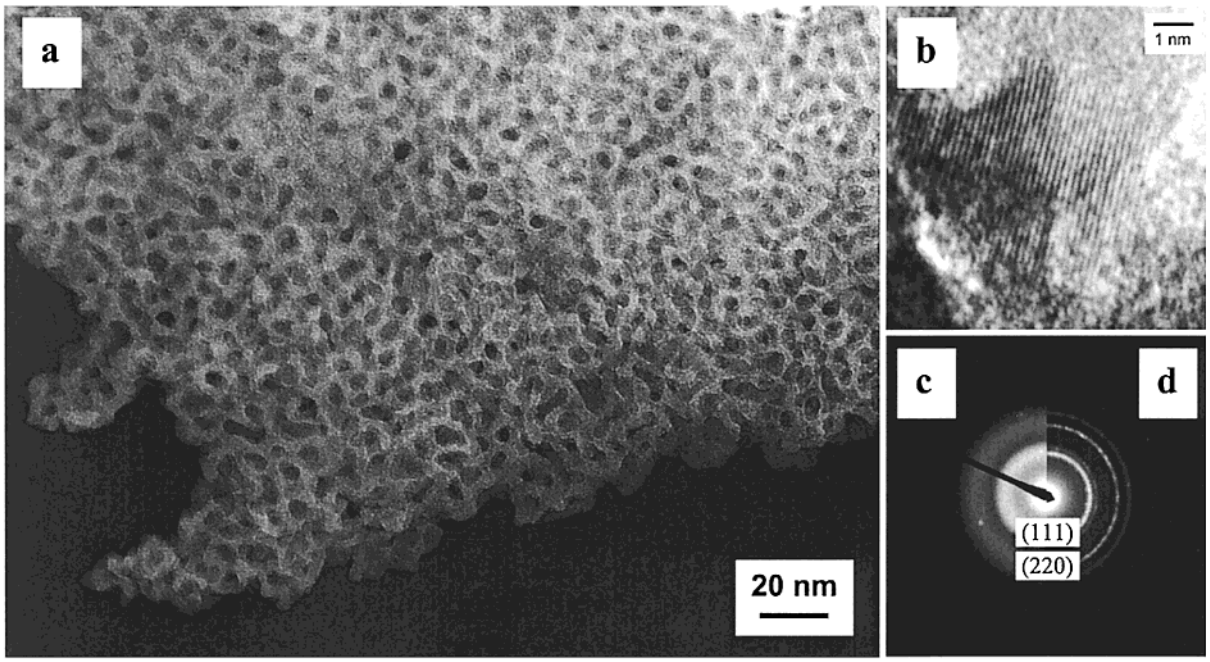

Figure 2. High-resolution TEM images of TMS14 materials prepared with colloid precursors: (a) WZr-TMS14 calcined at 600 °C under air (the sample was embedded in epoxy resin and microtomed into sections ~150 Å thick) and (b) pore wall of WZr-TMS14, shown under higher magnification. Also shown are the electron diffraction patterns of (c) WZr-TMS14 calcined at 600 °C and (d) the zirconia nanoparticle precursor. The studies were done on a JEOL 2010 transmission electron microscope equipped with a LaB_6 gun, operating at 200 kV.

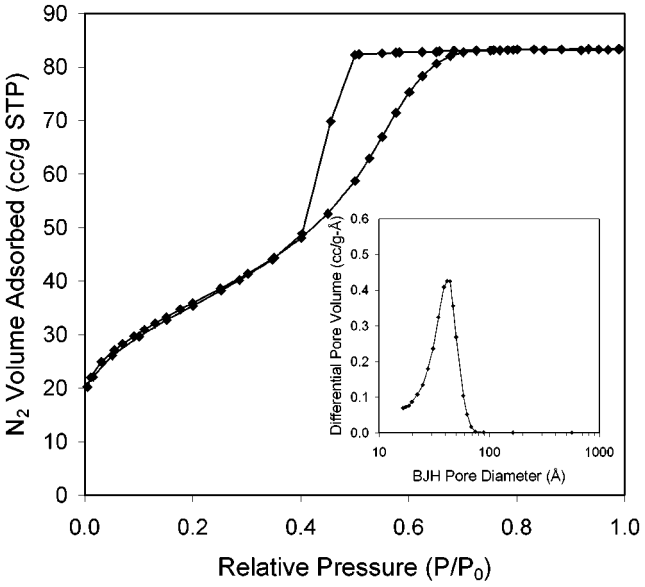

Figure 3. N_2 adsorption−desorption isotherm of WZr-TMS14 prepared with colloidal ZrO_2 precursor, and calcined at 600 °C under air. The sample was degassed at 150 °C under vacuum until a final pressure of 1×10^{-3} Torr was reached. The isotherm was then obtained at 77 K on a Micromeritics ASAP 2010 gas sorption and porosimetry system. The mesopore size distribution (inset) was calculated from the adsorption branch of the isotherm using the BJH (Barrett−Joyner−Halenda) method.

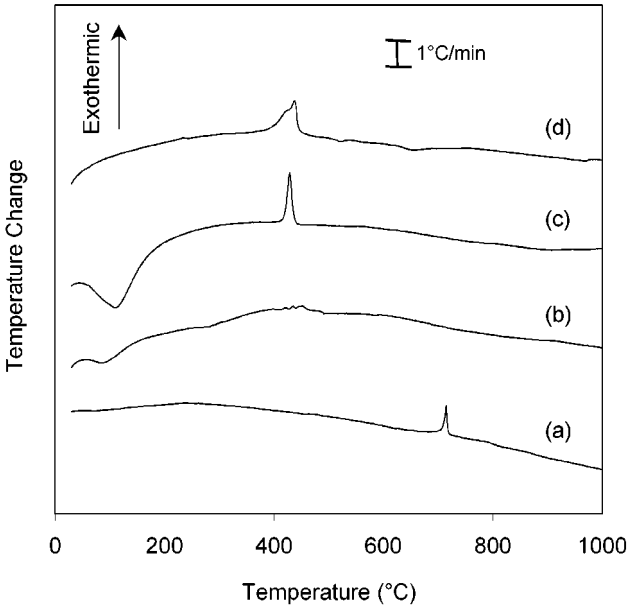

Figure 4. DTA profiles of (a) WZr-TMS14 calcined at 600 °C, (b) dried zirconia colloid particles, (c) hydrous zirconium oxide, and (d) hydrous tungsten oxide. Profiles were weight-normalized. DTA was performed on a Perkin-Elmer Series 7 thermal analysis system, using purified air as the flowing purge gas (~60 sccm) with a ramp rate of 5 °C/min. α-Al_2O_3 was used as the reference sample.

structure of WZr-TMS14, as indicated by XRD and nitrogen adsorption analyses of the materials calcined at 800 °C. WZr-TMS14 was nearly 300 °C more stable than the amorphous forms of its component metal oxides (Figures 4c and d), which crystallized around 430 °C. WZr-TMS14 was also more stable than the zirconia nanoparticle precursors (which exhibited a series of small exothermic peaks in the range of 410−470 °C (Figure 4b)).

WZr-TMS14 was found to contain 30.5 wt % WO_3 in the bulk (according to elemental analysis). Since tungsten oxide was not detected in the 600 °C-calcined material as a separate crystalline phase according to XRD and TEM results, it must

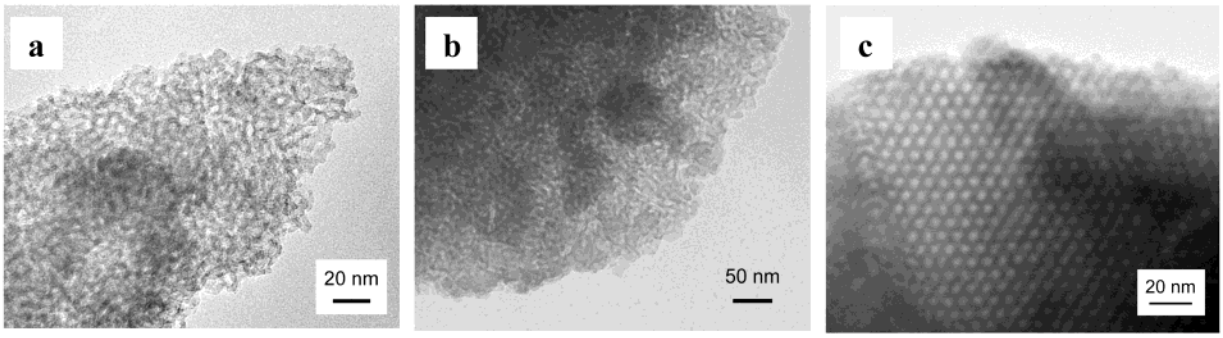

Figure 5. TEM images of (a) WTi-TMS14 calcined at 400 °C under air, (b) WAl-TMS14 calcined at 400 °C under air, and (c) WZr-TMS14 prepared with $ZrO(NO_3)_2$ salt and calcined at 250 °C under nitrogen.

be highly dispersed throughout the framework. The tungsten oxide may be viewed as being distributed as a coating on the discrete zirconia nanoparticles that make up the mesoporous framework.

WZr-TMS14 had a measured BET surface area of 130 m^2/g, a value surprisingly close to the maximum theoretical surface area for a model structure composed of hard spheres (surface area = $6000/\rho D$, where ρ and D are the density (cm^3/g) and diameter (nm) of the spherical particle, respectively). As a rough approximation, the hard spheres were modeled as 5-nm cubic zirconia particles covered by a layer of tungsten oxide (such that the total content was 30.5 wt % WO_3). Higher surface areas in WZr-TMS14 could be possible by using smaller nanoparticles or by incorporating microporosity into the pore walls. For comparison, mesoporous SBA-15 silicas (prepared using the same Pluronic surfactant) have pore sizes of 4.7−8.9 nm, pore walls of 3.1−6.4 nm, and surface areas of 800 m^2/g and higher, depending on aging conditions.[4] It has been shown that SBA-15 contains micropores in the pore walls, which were formed from the removal of deeply occluded Pluronic surfactant poly(ethylene oxide) chains; micropores are known to contribute significantly to the measured surface area.[20] WZr-TMS14 did not contain microporosity, as determined through nitrogen adsorption measurements.

The WZr-TMS14 surface composition was enriched in tungsten; a surface W/Zr value of 1.44 was determined through X-ray photoelectron spectroscopy, substantially exceeding the bulk-average W/Zr value of 0.23 (= 30.5 wt % WO_3). The tungsten surface species conferred Lewis and Brønsted acidity to WZr-TMS14 as detected via pyridine adsorption diffuse reflectance Fourier-transform infrared spectroscopy. Preliminary data indicated that WZr-TMS14 was catalytically active for various hydrocarbon gas-phase reactions, such as isomerization and cracking.[21] WZr-TMS14 could be considered a new form of tungstated zirconia solid acid catalysts, which are conventionally prepared through impregnation or co-precipitation methods.[22] Inorganic colloidal particles have been studied previously for the preparation of thermally stable catalysts in which porosity arises from interparticle voids rather than from the removal of a surfactant template.[23]

We propose that mesostructure formation occurs through $(S^0H^+)(I^-C^+)$ charge interactions that lead to the cooperative assembly of the nanoparticle/surfactant mesostructure. This synthesis pathway has been discussed for SBA-15,[4] but very different "chemical" species are involved for WZr-TMS14 formation. Attractive forces among the charged precursors (namely, metatungstate anions (I^-), positively charged colloid nanoparticles (C^+) and the hydrogen-bonded polymer surfactants (S^0H^+)) are believed to be the prevailing mode of interaction at the low pH conditions employed. The solubilized triblock copolymer surfactant aggregates into micelles containing a hydrophobic poly(propylene oxide) (PPO) micellar core and a hydrophilic poly(ethylene oxide) (PEO) corona. The PEO corona can hydrogen-bond with hydrated protons $[H_3O]^+$ under acidic conditions as observed with poly(ethylene glycol) (which is composed exclusively of EO units).[24] In this manner, the triblock copolymer micelles can effectively assume a net positive charge and participate in the electrostatic assembly of WZr-TMS14. A chelating interaction of the EO blocks (of the triblock copolymer surfactant) with metal cations in a nonaqueous environment was proposed by Yang et al. in a different synthesis method,[11] but such interaction can be disrupted by water[25] and is therefore not thought to play an important role in the aqueous-route formation of the TMS14 materials.

The zirconia nanoparticles were positively charged, since the pH of the sol (~0.5) was below the point-of-zero charge (pzc) of zirconia (pzc ~ 4−6).[26] The nanoparticles were stabilized by a layer of nitrate counteranions and remained completely in suspension because of the electrostatic repulsion of their electrical double layers.[27] It is known that particle suspensions could be forced to coagulate by adding salts such as a tungstate salt, but no reaction was observed when the ZrO_2 sol was combined with AWO; the Pluronic surfactant was needed to induce a reaction. In addition, precipitation of WZr-TMS14 did not occur when the tungstate salt was withheld from the synthesis mixture. The presence of all three components was critical to the WZr-TMS14 mesostructure formation.

Nanoparticles of another composition were used to test the versatility of this synthesis pathway. Titania nanoparticles (size ~4−6 nm) were produced via controlled hydrolysis of titanium chloride (Aldrich).[28] The sol pH was adjusted to <1 and an equivalent metal oxide amount was added to the AWO/surfactant solution. Calcination at 400 °C led to a mesoporous tungstated titania WTi-TMS14 (Figure 5a) which

had a surface area of 168 m^2/g and a pore size of 4.3 nm. WTi-TMS14 exhibited a weak SAXS pattern similar to that of WZr-TMS14, before and after calcination. It can also be calcined at 600 °C while retaining the mesoporous framework with a lower surface area (68 m^2/g), but a separate tungsten oxide phase was found.

Metal oxo clusters in the form of an aluminum Keggin ion ("Al_{13}", $[AlO_4Al_{12}(OH)_{24}(H_2O)_{12}]^{7+}$ [29]) were studied as the metal oxide precursor to tungstated alumina. A solution of Al_{13} was prepared according to published procedures,[29] and an equivalent metal oxide amount was added to the synthesis solution. Calcination at 400 °C also led to a mesoporous material (Figure 5b). WAl-TMS14 had a surface area of 134 m^2/g and a pore size of 6.7 nm. The pores were larger than expected but may have been due to a different synthesis pH used (~5), associated with the Al_{13} solution; corresponding to the larger pores was a larger Bragg spacing (10.9 nm). The mesoporous structure was lost when the material was calcined at 600 °C. It is noted that other researchers have reported using Al_{13} as a precursor to mesoporous alumina[30] and aluminophosphates.[14] Other molecular clusters, such as $Ti_{16}O_{16}(OEt)_{32}$,[31] $Ge_4S_{10}^{4-}$,[32] and $SnSe_4^{4-}$,[33] have been used successfully to produce well-ordered organic−inorganic mesostructures, but so far these mesostructures have been unstable to surfactant removal.

That the nanoparticle form of the precursor was found not necessary for mesostructure formation suggested that metal salt precursors could also be used. In fact, an ordered WZr-TMS14 mesostructure was prepared by using $ZrO(NO_3)_2$ salt (Figure 1b) instead of zirconia nanoparticles. It exhibited regions of well-ordered hexagonal packing (Figure 5c), which were not detected in materials prepared with nanoparticles. The salt-derived WZr-TMS14 was mesoporous and had a surface area of 80 m^2/g after calcination at 250 °C under nitrogen. However, there was a loss of long-range ordering (Figure 1b, trace V) and reduction of surface area to 4 m^2/g after calcination at 600 °C. Both nanoparticle and salt precursors led to mesoporous materials, but the use of the colloidal form provided much greater thermal stability.

WZr-TMS14 prepared with the zirconium salt was found to have a bulk W/Zr molar ratio (2.45) significantly higher than that prepared with zirconia nanoparticles (0.23). A lower stability could be due to the higher concentration of tungsten oxide, to thinner pore walls, to the lack of crystallinity in the zirconia domains, or to a combination of these effects. WTi-TMS14 and WAl-TMS14 had W/metal ratios of 0.90 and 0.48, respectively, giving credence that having a relatively low W amount in these tungstated metal oxides (regardless of metal precursor form) was desirable for stability of the mesoporous framework.

In conclusion, a novel supramolecular templating approach to thermally stable, crystalline mesoporous nanocomposites has been successfully demonstrated using discrete inorganic nanoparticles as "preformed" building blocks. This nanoparticle/surfactant templating route can accommodate nanoparticles of different sizes and compositions, with the resulting mesostructured material retaining the characteristics of the constituent particles. Favorable charge interactions among nanoparticles, micellar aggregates, and tungstate salts likely explain the formation of the TMS14 mesostructures. Positively charged metal oxo clusters and metal salts were also found to produce mesostructures. Calcination of all these supramolecular-templated mesostructures yielded mesoporous materials with high surface areas. The mesoporous tungstated metal oxides prepared with nanoparticles were thermally robust. The nanoparticle/surfactant templating methodology appears quite general and should be adaptable to other types of nanoparticulate systems, as well as to other types of surfactants and oxometalate anions.

Acknowledgment. The authors thank C.-C. Wang and W. Rupp (MIT) for the colloid sol precursors, Nyacol (Valley Forge, PA) for the colloidal zirconia, and BASF (Mt. Olive, NJ) for the copolymer surfactants. The authors are grateful to M. Frongillo (MIT/NSF Center for Materials Science and Engineering) for assistance with electron microscopy. This work was supported by the David and Lucile Packard Foundation and the Office of Naval Research.

References

(1) Kresge, C. T.; Leonowicz, M. E.; Roth, W. J.; Vartuli, J. C.; Beck, J. S. *Nature* **1992**, *359*, 710.
(2) Ying, J. Y.; Mehnert, C. P.; Wong, M. S. *Angew. Chem., Int. Ed. Engl.* **1999**, *38*, 56.
(3) Huo, Q.; Margolese, D. I.; Ciesla, U.; Feng, P.; Gier, T. E.; Sieger, P.; Leon, R.; Petroff, P. M.; Schüth, F.; Stucky, G. D. *Nature* **1994**, *368*, 317.
(4) Zhao, D.; Feng, J.; Huo, Q.; Melosh, N.; Fredrickson, G. H.; Chmelka, B. F.; Stucky, G. D. *Science* **1998**, *279*, 548.
(5) Tanev, P. T.; Pinnavaia, T. J. *Science* **1995**, *267*, 865.
(6) Bagshaw, S. A.; Prouzet, E.; Pinnavaia, T. J. *Science* **1995**, *269*, 1242.
(7) Kageyama, K.; Tamazawa, J.; Aida, T. *Science* **1999**, *285*, 2113.
(8) Yang, P.; Wirnsberger, G.; Huang, H. C.; Cordero, S. R.; McGehee, M. D.; Scott, B.; Deng, T.; Whitesides, G. M.; Chmelka, B. F.; Buratto, S. K.; Stucky, G. D. *Science* **2000**, *287*, 465.
(9) Antonelli, D. M.; Ying, J. Y. *Angew. Chem., Int. Ed. Engl.* **1995**, *34*, 2014.
(10) Antonelli, D. M.; Ying, J. Y. *Angew. Chem., Int. Ed. Engl.* **1996**, *35*, 426. (b) Antonelli, D. M.; Nakahira, A.; Ying, J. Y. *Inorg. Chem.* **1996**, *35*, 3126. (c) Antonelli, D. M.; Ying, J. Y. *Chem. Mater.* **1996**, *8*, 874.
(11) Yang, P.; Zhao, D.; Margolese, D. I.; Chmelka, B. F.; Stucky, G. D. *Nature* **1998**, *396*, 152.
(12) Ciesla, U.; Schacht, S.; Stucky, G. D.; Unger, K. K.; Schüth, F. *Angew. Chem., Int. Ed. Engl.* **1996**, *35*, 541.
(13) Wong, M. S.; Ying, J. Y. *Chem. Mater.* **1998**, *10*, 2067.
(14) Holland, B. T.; Isbester, P. K.; Blanford, C. F.; Munson, E. J.; Stein, A. *J. Am. Chem. Soc.* **1997**, *119*, 6796.
(15) Satterfield, C. N. *Heterogeneous Catalysis in Industrial Practice*, 2nd ed.; McGraw-Hill: New York, 1991.
(16) Stein, A.; Fendorf, M.; Jarvie, T. P.; Mueller, K. T.; Benesi, A. J.; Mallouk, T. E. *Chem. Mater.* **1995**, *7*, 304.
(17) Elder, S. H.; Gao, Y.; Li, X.; Liu, J.; McCready, D. E.; Windisch, C. F., Jr. *Chem. Mater.* **1998**, *10*, 3140.
(18) Ryoo, R.; Kim, J. M.; Ko, C. H.; Shin, C. H. *J. Phys. Chem.* **1996**, *100*, 17718.
(19) Carrier, X.; d'Espinose de la Caillerie, J.-B.; Lambert, J.-F.; Che, M. *J. Am. Chem. Soc.* **1999**, *121*, 3377.
(20) Impéror-Clerc, M.; Davidson, P.; Davidson, A. *J. Am. Chem. Soc.* **2000**, *122*, 11925.
(21) Wong, M. S.; Jehng, J.-M.; Wachs, I. E.; Ying, J. Y., in preparation.
(22) Santiesteban, J. G.; Vartuli, J. C.; Han, S.; Bastian, R. D.; Chang, C. D. *J. Catal.* **1997**, *168*, 431.
(23) Murrell, L. L. *Catal. Today* **1997**, *35*, 225.
(24) Bailey, F. E., Jr.; Callard, R. W. *J. Appl. Polym. Sci.* **1959**, *1*, 56.
(25) Okada, T. *Analyst* **1993**, *118*, 959.
(26) Parks, G. A. *Chem. Rev.* **1965**, *65*, 177.
(27) Rajagopalan, R.; Heimenz, P. C. *Principles of Colloid and Surface Chemistry*, 3rd ed.; Marcel Dekker: New York, 1997.

(28) Rajh, T.; Ostafin, A. E.; Micic, O. I.; Tiede, D. M.; Thurnauer, M. C. *J. Phys. Chem.* **1996**, *100*, 4538.
(29) Kloprogge, J. T.; Seykens, D.; Jansen, J. B. H.; Geus, J. W. *J. Non.-Cryst. Solids* **1992**, *142*, 94.
(30) Valange, S.; Guth, J.-L.; Kolenda, F.; Lacombe, S.; Gabelica, Z. *Microporous Mesoporous Mater.* **2000**, *36*, 597.
(31) Soler-Illia, G. J.; Scolan, E.; Louis, A.; Albouy, P.; Sanchez, C. *New J. Chem.* **2001**, *25*, 156.
(32) MacLachlan, M. J.; Coombs, N.; Ozin, G. A. *Nature* **1999**, *397*, 681.
(33) Trikalitis, P. N.; Rangan, K. K.; Bakas, T.; Kanatzidis, M. G. *Nature* **2001**, *410*, 671.

NL015594Y